# Overview of computational advances in Quantitative Phase Imaging using Digital Holographic Microscopy

A. Doblas<sup>a</sup>, B. Bogue-Jimenez<sup>a</sup>, S. Obando-Vasquez<sup>b</sup>, R. Castañeda<sup>b</sup>, and C. Trujillo<sup>b</sup>
<sup>a</sup>Department of Electrical and Computer Engineering, UMass – Dartmouth, U.S.A
<sup>b</sup> Applied Sciences and Engineering school, Universidad EAFIT, Medellin, Colombia.

## **ABSTRACT**

Owing to its high resolution, sensitivity, imaged field of view, and frame rate acquisition, Digital Holographic Microscopy (DHM) stands out among the Quantitative phase imaging (QPI) techniques to reconstruct high-resolution phase images from micrometer-sized samples, providing information about the sample's topography and refractive index. Despite the successful performance of DHM systems, their applicability to in-situ clinical research has been partially hampered by the need for a standard phase reconstruction algorithm that provides quantitative phase distributions without any phase distortion. This invited talk overviews the current advances in computational DHM reconstruction approaches from semi-heuristic to learning-based approaches.

**Keywords:** Digital Holographic Microscopy, phase shifting, off-axis, angular spectrum, phase compensation.

## 1. INTRODUCTION

Quantitative phase imaging (QPI) techniques are a class of imaging methods used to measure the phase shift of light as it passes through or interacts with a sample[1]. These techniques provide quantitative information about the optical properties of the sample, such as refractive index variations and thickness, which are not readily accessible with conventional intensity-based imaging[2].

Among QPI techniques, Digital Holographic Microscopy (DHM) stands out for its high resolution, sensitivity, wide field of view, and fast acquisition rates [3,4]. Over the past decade, DHM has matured significantly, thanks to extensive research on its optical design, phase reconstruction algorithms, and diverse applications in life and materials sciences [5–7]. In general, DHM can be implemented in two types of configurations: In-line DHM and off-axis DHM. Off-axis DHM improves the reconstruction bandwidth of complex wavefronts by suppressing the object autocorrelation. It also offers improved capabilities in quantitative phase imaging, single-shot capability, and easy implementation in conventional white-light microscopes[8]. In contrast, in-line DHM provides fast 3D images with improved accuracy, reduced noise, and reduced computational complexity compared to direct methods and iterative methods[9].

Despite its success, DHM's widespread adoption in clinical research faces obstacles due to the absence of a standardized computational framework. This lack hinders the generation of distortion-free quantitative phase maps with minimal user input, crucial for real-time clinical applications [10,11]. To address this gap, our collaborative effort aims to enhance the computational framework of DHM technology. This paper presents a practical guide for implementing a computational DHM framework based on the optical setup of DHM systems, utilizing publicly available computational algorithms. Our objective is to simplify DHM usage, making it more accessible and user-friendly, thereby facilitating its integration into clinical research and practical applications.

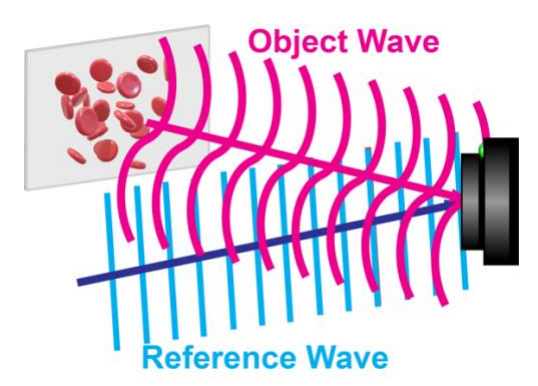


Fig. 1. Scheme of a DHM system based on the optical interference between two coherent waves (i.e., the object and reference waves).

## 2. DIGITAL HOLOGRAPHIC MICROSCOPY

DHM systems (Fig. 1) are optical interferometers that generate two mutually coherent interfering wavefronts – the object and reference wavefronts[4]. The reference wavefront is uniform and planar, while the object wavefront encodes the complex amplitude distribution scattered by a microscopic sample. The object wavefront is then imaged through a native optical microscope positioned in one of the interferometer arms onto the output plane of the system, which is also the sensor plane of the digital camera. In general, the native optical microscope comprises an infinity-corrected microscopic objective (MO) lens and a converging tube lens (TL), which produce an in-focus image  $[u_{\rm IP}(x,y)]$  of the microscopic sample when the object is positioned at the working distance of the MO lens.

$$u_{IP}(x,y) = \frac{1}{M^2} \exp\left(j\frac{k}{2C}(x^2 + y^2)\right) \times \left[o\left(\frac{x}{M}, \frac{y}{M}\right) \otimes_2 P\left(\frac{x}{\lambda f_{TL}}, \frac{y}{\lambda f_{TL}}\right)\right]. \tag{1}$$

In Eq. (1),  $k = 2\pi/\lambda$  is the illumination wavenumber,  $\bigotimes_2$  denotes the 2D convolution operator,  $M = -f_{TL}/f_{MO}$  is the lateral magnification of the microscopic imaging system, which depends on the ratio between the focal lengths of the MO and TL lenses, respectively. The in-focus complex amplitude distribution is the product of a quadratic phase term and the 2D convolution between a scaled replica of the complex object distribution [i.e., o(x,y)] and a scaled replica of the 2D Fourier transform of the pupil transmittance [i.e.,  $P(u,v) = FT\{p(x,y)\}$ ]. The pupil has been considered to be located at the back focal plane of the MO lens[12]. In Eq. (1), the radius of curvature of the quadratic phase term depends on the optical configuration of the microscopic imaging system[13]. In particular, its value is inversely proportional to the difference between the focal length of the TL lens ( $f_{TL}$ ) and the axial distance between the pupil and TL planes (d),  $C = \frac{f_{TL}^2}{f_{TL}-d}$ . The maximum value of C (i.e.,  $C = \infty$ ) is found when the pupil is located at the front focal plane of the TL lens (i.e.,  $d = f_{TL}$ ), assembling the imaging system in the telecentric regime[13]. Under the telecentric condition (i.e.,  $d = f_{TL}$ ), the quadratic phase factor in Eq. (1) is optically removed.

The sensor in a DHM system records the irradiance distribution of the coherent superposition between the object and reference wavefronts, commonly called digital hologram. Without loss of generality, the object wave can be considered as the out-of-focus complex wavefield produced by the microscope at a distance z from the image plane [13].

$$u(x, y; z) = u_{IP}(x, y) \otimes_2 \exp\left(j\frac{k}{2z}(x^2 + y^2)\right).$$
 (2)

For simplicity, we have neglected some constant factors in Eq. (2). Assuming that the complex amplitude distribution of the reference wave is a titled plane wavefront,  $r(x,y) = \sqrt{I_R} \exp\left[jk(sin\theta_x \cdot x + sin\theta_y \cdot y)\right]$  where  $I_R$  is the irradiance of the reference wavefront, and  $\theta = (\theta_x, \theta_y)$  is the vector representation of the titled reference angle to the optical axis, the irradiance distribution of the hologram, h(x,y;z) is

$$h(x, y; z) = |u(x, y; z)|^2 + |r(x, y)|^2 + u(x, y; z)r^*(x, y) + u^*(x, y; z)r(x, y),$$
(3)

where  $|\cdot|^2$  and \* are the square module and complex conjugate operator, respectively. The irradiance distribution of the hologram is the sum of four terms: the object irradiance [i.e.,  $|u|^2$ ], the reference irradiance [i.e.,  $|r|^2$ ], the real image [i.e.,  $u^*r^*$ ], and the virtual one [i.e.,  $u^*r^*$ ].

## 3. COMPUTATIONAL DHM FRAMEWORK

Equation (3) shows that the object information o(x,y), encoded in u(x,y;z), is mixed with other three terms, requiring a computational algorithm to separate these three terms from the object information and reconstruct the complex in-focus amplitude distribution [Eq. (1)] with minimum distortions. The selection of the computational DHM algorithm depends on the system's optical configuration. The user must know the following questions to select the algorithm: 1) does the system operate in an off-axis, slightly off-axis or in-line configuration?[10]; 2) does the system operate in a telecentric or non-telecentric regime?[11]; and 3) is the sensor placed at the image plane?[12]. Figure 2 shows a flowchart to select the computational algorithm based on the answers to these questions. We recognize that users of a DHM system may not know the answers to these questions, however any individual can answer these questions by analyzing and observing the Fourier Transform of the hologram distribution [Eq. (3)]. The 2D Fourier transform of the hologram, H(u,v;z) can be mathematically represented as

$$H(u,v;z) = DC(u,v;z) + U\left(u - \frac{\sin\theta_x}{\lambda}, v - \frac{\sin\theta_y}{\lambda}; z\right) + U^*\left(u + \frac{\sin\theta_x}{\lambda}, v + \frac{\sin\theta_y}{\lambda}; z\right), \tag{4}$$

where (u,v) are the transverse spatial frequencies, and  $DC(u,v;z) = U \otimes_2 U^* + R \otimes_2 R^*$ . In Eq. (4), we have considered that the reference wavefront is a plane wavefront, which is a standard assumption in DHM setups. The capital letters refer to the 2D Fourier transform distributions to simplify our notation. Equation (4) shows that the hologram's spectrum consists of three terms: DC, +1 [i.e., U(·)], and -1 [i.e., U\*(·)] terms. Whereas the DC term is always placed at the center of the hologram spectrum, the center positions of the  $\pm 1$  terms vary depending on the interference angle  $\theta$ =( $\theta_x$ , $\theta_y$ ) between the object and reference waves. This means that the  $\pm 1$  terms may overlap with the DC term on the hologram's spectrum if the interference angle between the two wavefronts is null or slightly small. In fact, the three terms in Eq. (4) entirely overlap [Fourier transform in Fig. 3(a)] if the DHM system operates in in-line (or on-axis) regime. Note that in-line DHM holograms do not present any interference fringes. The reconstruction algorithm for in-line DHM systems is based on phase-shifting (PS) techniques, requiring the acquisition of multiple holograms in which the phase of the reference wavefront shifts (e.g., phase-shifted holograms)[14–17]. Traditionally, PS algorithms require five, four, and three phase-shifted holograms among the different PS algorithms[10]. In the five- and four-step algorithms, the phase shift between the holograms is  $\pi/2$ , reconstructed phase images by

$$\varphi(x,y) = \tan^{-1} \left( \frac{2[h(x,y;3\pi/2)] - h(x,y;\pi/2)}{2h(x,y;\pi) - h(x,y;0) - h(x,y;2\pi)} \right),$$
 (5)

and

$$\varphi(x,y) = \tan^{-1} \left( \frac{h(x,y;3\pi/2) - h(x,y;\pi/2)}{h(x,y;\pi) - h(x,y;0)} \right), \tag{6}$$

using five and four phase-shifted holograms, respectively. The third variable of the hologram distribution in Eqs. (5) and (6) denotes the phase shift of the reference wavefront. For example,  $h(x,y;\pi)$  is a recorded hologram in which there is a phase shift of  $\pi$  to the first hologram. The number of phase-shifted holograms can be reduced to three if the phase shift between holograms is  $2\pi/3$ . Consequently, the reconstructed phase distribution with the three phase-shifted holograms is obtained by

$$\varphi(x,y) = \tan^{-1} \left( \sqrt{3} \frac{h(x,y;5\pi/3) - h(x,y;\pi/3)}{h(x,y;5\pi/3) - h(x,y;\pi/3) - 2h(x,y;\pi)} \right). \tag{7}$$

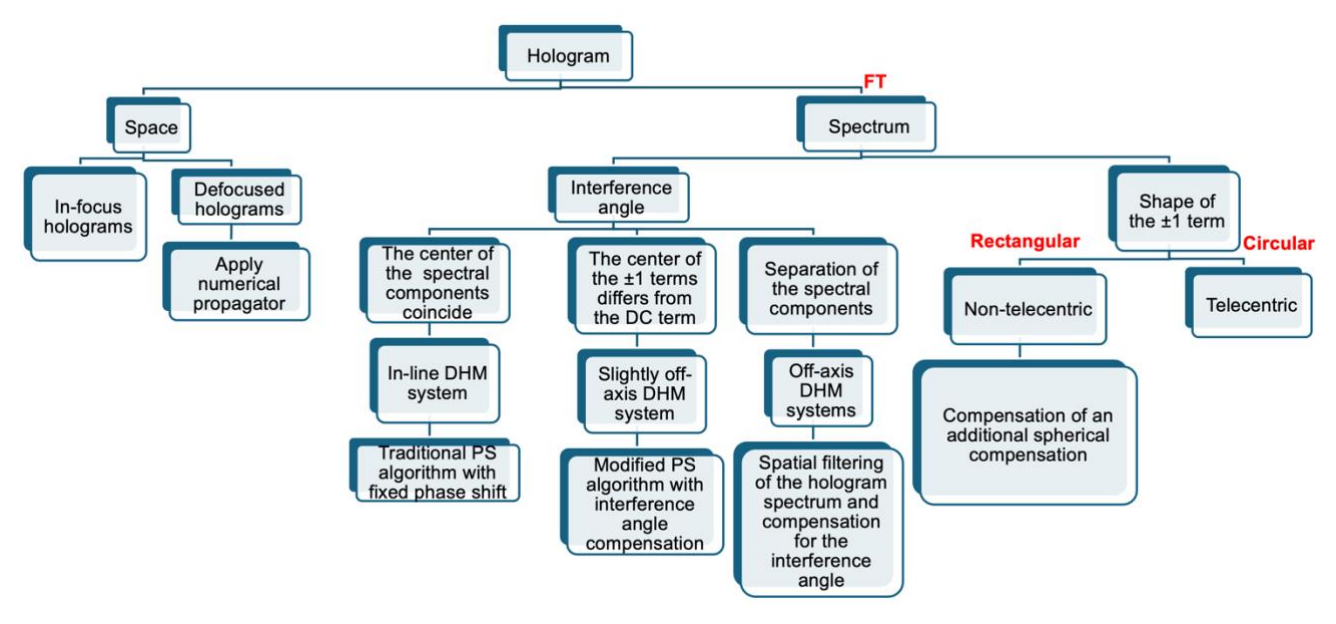


Fig. 2. Analysis of the hologram and its spectrum to select the correct computational DHM algorithm to reconstruct accurate quantitative phase images.

Reducing the number of required phase-shifted holograms presents a tradeoff between acquisition time and noise sensitivity. Whereas fewer holograms make the algorithm more suitable for dynamic imaging, the reconstructed phase maps are more sensitive to noise [18]. Nonetheless, the main advantage of these three PS algorithms [Eqs. (5)-(7)] is the computational efficiency since the reconstructed phase images are obtained via point-wise subtractions and division operations between the digitally recorded phase-shifted holograms.

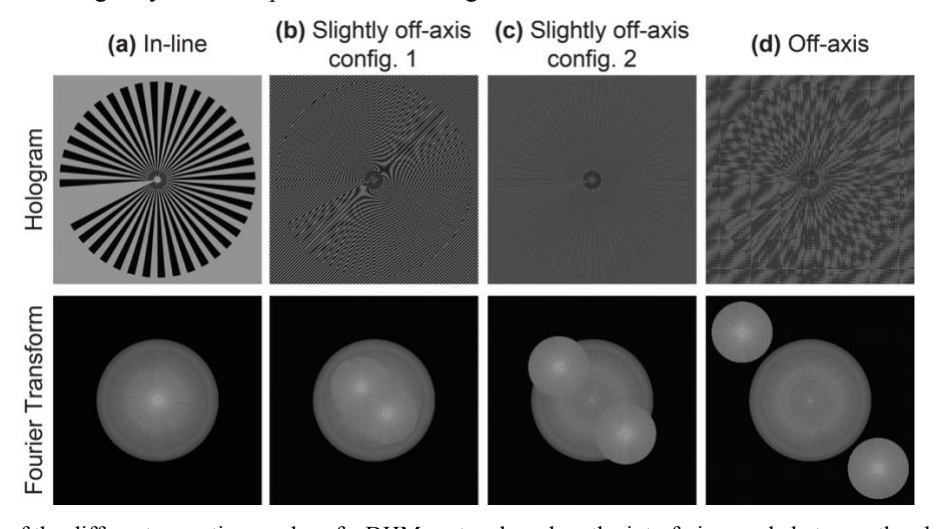


Fig. 3. Illustration of the different operating modes of a DHM system based on the interfering angle between the object and reference wavefronts.

Setting up in-line DHM systems is nearly impossible since experimental holograms always exhibit residual interferential fringes due to aberrations of the optical components. Slightly off-axis DHM systems are characterized by holograms with interferential fringes featuring low spatial frequency[15]. This indicates partial overlapping between the DC term and  $\pm 1$  terms on the hologram's spectrum. Figure 3(b) shows two different slight off-axis DHM systems in which the interference angle varies. Although multiple phase-shifted holograms and a PS algorithm are still required to reconstruct phase

distributions in slightly off-axis DHM systems, there is also a need to compensate for the interference angle between the object and reference wavefronts. In 2002, De Nicola et al. reconstructed the complex amplitude distribution of an object by summing the individual products between the recorded phase-shifted holograms with a phase shift of  $\pi/2$  and their corresponding digital reference wavefronts[19],

$$\hat{u}(x,y) = h(x,y;0)\hat{r}(x,y;0) + h(x,y;\pi/2)\hat{r}(x,y;\pi/2) +h(x,y;\pi)\hat{r}(x,y;\pi) + h(x,y;3\pi/2)\hat{r}(x,y;3\pi/2).$$
(8)

From Eq. (8), one can reconstruct both the amplitude and phase images via  $|\hat{u}(x,y)|$  and  $atan(imag[\hat{u}(x,y)], real[\hat{u}(x,y)])$ , respectively.

The PS algorithms in Eqs. (5) - (8) require a constant and fixed phase shift between the recorded holograms, demanding accurate optical components to achieve such phase shifts and DHM systems with high temporal stability [15,16]. Blind PS strategies have been proposed to have multiple holograms with a random and unknown phase shift. Among the different blind PS approaches, we proposed two blind iterative PS approaches for slightly off-axis DHM systems [17,20]. Both blind PS methods are based on the correct separation of the three different composing the hologram's spectrum, Eq. (4). In the first blind PS method, the hologram distribution [Eq. (3)] is given by a linear combination of three components {d<sub>0</sub>, d<sub>+1</sub> and  $d_{-1}$ } where  $d_0$  is the first two terms of Eq. (3), and  $d_{+1}$  and  $d_{-1}$  are, respectively, the third and fourth terms. In particular,  $d_{+1} = u(x, y; z)e^{-jk\sin\theta \cdot x}$ , and  $d_{-1} = u^*(x, y; z)e^{jk\sin\theta \cdot x}$ . Note that each component in Eq. (3) has a different weighting depending on the phase shift ( $\Delta\theta$ ),  $h = d_0 + e^{-j\Delta\theta} d_{-1} + e^{j\Delta\theta} d_{-1}$ . The separation of complex object information can be reconstructed by estimating  $d_{+1}$  distribution as a linear system's equation using three recorded holograms,  $\{h_1, h_2, h_3\}$  with arbitrary phase shifts  $\{\Delta\theta_1, \Delta\theta_2, \Delta\theta_3\}$ . Accurately estimating the  $d_{+1}$  term requires the correct values of the phase shifts between the holograms. If the values of the phase shifts are incorrect (i.e., they do not coincide with the experimental ones), the spectrum of the  $d_{+1}$  component,  $D_{+1}$ = FT[ $d_{+1}$ ], presents two frequency peaks. Our blind 3-step PS approach simultaneously estimates the phase shifts between the holograms,  $\{\Delta\theta_1, \Delta\theta_2, \Delta\theta_3\}$ , and the complex  $d_{+1}$  distribution by analyzing the spectral components of  $D_{+1}$  and ensuring that the spectrum  $D_{+1}$  distribution is unique (i.e., it only has a unique frequency peak). Estimating the phase shifts and the  $d_{+1}$  component is provided by minimizing a cost function that quantifies the difference between the absolute value of the  $D_{+1}$  component in the real and residual peaks. Reference [17] provides more details of the blind 3-step PS algorithm. Once the d+1 term is calculated, the amplitude image is obtained as  $|d_{+1}(x,y)|$ , and the phase image is obtained as the angle of the product between  $d_{+1}$  and a digital reference wave,  $\varphi = \text{angle}[d_{+1} \cdot r_D]$  The second PS algorithm[20], which only requires two phase-shifted holograms, is only suitable for slightly off-axis DHM systems in which the spectra of the d<sub>+1</sub> and d<sub>-1</sub> terms do not overlap in the Fourier domain, see Fig. 3(b). Under this condition, the hologram can be written as the sum of two components  $\{d_0, d_2\}$  as  $h = d_0 + e^{j\Delta\theta} d_2$  where  $d_2$  $= d_{+1} + e^{-j2\Delta\theta} d_{-1}$  [ref]. Similarly to the blind 3-step approach, the  $d_2$  component and phase shift between both holograms are estimated by minimizing a cost function that focuses on the uniqueness of the spectrum of the  $d_0$  component. Because the spectrum of  $d_2$  component is composed of the spectrums of  $d_{-1}$  and  $d_{-1}$ , one must filter the spectral frequencies of the  $d_{+1}$ term and multiply the filtered  $d_{+1}$  term with a replica of the reference wavefront to reconstruct the phase distribution. Whereas the previous PS algorithms were linear, the blind 2-step PS method is not since it requires a spatial filter to retrieve the  $d_{+1}$  term. An important limitation of both blind PS approaches [17,20] is that they only work for DHM systems operating in telecentric regime since the center of the ±1 terms in the Fourier transform should correspond to a maximum peak. A priori, the traditional known-phase PS algorithms [Eqs. (5)-(8)] can be used for both non-telecentric- and telecentric-based DHM systems, noting that the reconstructed phase distribution is distorted by a spherical wavefront. Such distortion should be compensated for accurate quantitative phase analysis. An automated approach is discussed above for compensating for this factor with minimum user input.

Both in-line and slightly off-axis DHM systems require multiple recorded holograms to implement the PS algorithm, limiting their dynamic imaging and analysis use. Off-axis DHM systems are the most suitable systems for real-time imaging since the complex object distribution can be reconstructed from a single hologram[21]. The spectral components in off-axis holograms are not superimposed [Fourier Transform in Fig. 3(c)] since the interfering angle between the interfering wavefronts is higher, generating interferential fringes of high spatial frequency. This means that the computational DHM framework for off-axis DHM systems consists of two main steps: (1) the spatial filtering of object spectrum located at the spatial frequencies  $(\sin\theta_x/\lambda, \sin\theta_y/\lambda)$ ,  $D_{+1} = U(u - \sin\theta_x/\lambda, v - \sin\theta_y/\lambda)$  [22], and (2) the phase compensation of the interfering angle between the object and reference wavefronts by multiplying  $h_F = IFT[H_F]$  with a digital reference wavefront,  $\hat{u}(x) = r_D(x)[H_F(x)]$ . [23]. Assuming that the wavelength of the light source and the features

of the digital sensor (i.e., number of pixels and their pitch) are well known, the generation of a digital plane reference wavefront requires the knowledge of the subtraction between the pixel locations of the DC and the +1 terms in the hologram spectrum [ref]. In particular, the only unknown parameter is the location of the +1 term. The determination of this parameter must be executed precisely to provide phase images without sawtooth fringes. In 2016, Trujillo et al. proposed an automated approach that finds the optimal non-integer pixel value of the maximum peak in the +1 term by searching for the optimal reconstructed phase image that presents the least number of phase discontinuities using nested loops[23]. In 2021, Castaneda et al. implemented a heuristic search of the non-integer pixel value of the +1 peak that provides the best reconstructed phase [24]. This heuristic algorithm finds the non-integer pixel corresponding to the minimum value of a cost function that tracks the number of phase jumps. Although the cost function presents a global minimum, sometimes it finds a local minimum, generating a reconstructed image that presents phase discontinuities. Last year, Obando-Vasquez et al. developed a semi-heuristic algorithm in which the search follows a path-oriented strategy, like the nested loop strategy [25], but with fewer steps. The proposed semi-heuristic algorithm is more time-efficient than the brute-forced search in Ref. [23], accurate reconstructed phase maps are provided 92x faster than the method using nested loops. On the other hand, comparing the heuristic and semi-heuristic approaches, the semi-heuristic approach produces more accurate phase measurements (i.e., lower standard deviation) and greater background stability between successive frames of the dynamic data, making it more suitable for video-rate quantitative phase imaging. In summary, although the three above off-axis reconstruction DHM algorithms look for the best reconstructed phase image via a summation-and-thresholding metric, their difference is how that search is performed.

As Eq. (1) shows, the reconstructed phase images in DHM systems operating in a non-telecentric regime are distorted by a quadratic phase factor that needs to be removed to provide accurate quantitative phase measurements [26]. Without prior information on the optical setup in a DHM system, one can easily identify its configuration (i.e., telecentric versus non-telecentric) by observing the shape of the  $\pm 1$  terms, see Fig. 4. The shape of the  $\pm 1$  terms in non-telecentric DHM systems is rectangular, see Fig. 4(a), compared to the circular one in telecentric DHM systems. In fact, the higher the rectangle, the smaller the radius of curvature C of the spherical wavefront in Eq. (1). The radius of curvature C for both lateral directions can be estimated knowing the maximum dimension of the  $\pm 1$  terms, the sensor's features (i.e., number of pixels and their pixel size) and the source's wavelength, see Eqs. (8) and (9) in Ref. [11]. In that work, Bogue-Jimenez et al. describe a computational tool for reconstructing accurate phase images in non-telecentric off-axis DHM systems based on previous work from Kemper's group [26]. An advantage of this non-tele DHM tool is that users only need to input two parameters (i.e., the sensor pixel size and source wavelength) to reconstruct phase images without distortions.

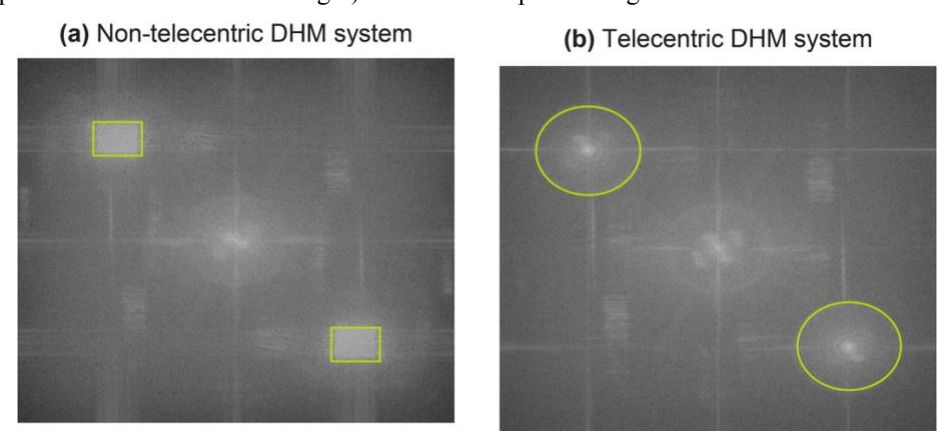


Fig. 4. The shape of the ±1 terms varies from rectangular to circular based on the optical configuration of the DHM imaging system.

Finally, DHM enables the 3D reconstruction of quantitative phase distributions from a defocused hologram by numerically propagating the reconstructed complex object wavefront, making DHM technology suitable for live cell imaging and 3D tracking applications [27,28]. This means that apart from the object's extraction information from the recorded hologram, the computational DHM framework should include numerical propagators based on the angular spectrum or Fresnel Transform approaches [29] to reconstruct the in-focus complex object distribution. Among the angular spectrum and Fresnel Transform approaches, the angular spectrum approach is the most common propagator in most DHM systems

because of its small propagation distance [30]. Assuming the angular spectrum approach, the in-focus complex amplitude distribution,  $\widehat{u}_{IP}(x,y)$ , is estimated as

$$\hat{u}_{IP}(x,y) = \text{IFT} \left[ \text{FT} \left[ \hat{u}(x,y;z_I) \right] \cdot \exp \left[ jkz_I \sqrt{1 - \lambda^2 (u^2 + v^2)} \right] \right], \tag{9}$$

where  $z_l z_l$  is the propagation distance,  $\hat{u}(x, y; z_l)$  is the reconstructed complex object amplitude distribution, and IFT[·] and FT[·] are the 2D inverse and direct Fourier transforms, respectively. From Eq. (9), the in-focus amplitude and phase object distributions are estimated by the absolute square modulus and the angle of Eq. (9), respectively. Last year, Castaneda et al. investigated a computational tool for reconstructing quantitative phase images from defocused holograms recorded in an off-axis telecentric-based DHM system using a heuristic framework [31]. This computational algorithm provides in-focus phase images without or with minimum phase distortions by minimizing a cost function that tracks the minimum value of the normalized variance in the reconstructed amplitude image and the minimum value of the phase jumps in the reconstructed phase image. This proposed computational tool was validated in static and dynamic defocused holograms and demonstrated superior performance to the traditional strategy in which the phase compensation of the interfering angle and the numerical focusing are performed sequentially. This method enables the automatic phase reconstruction of defocused holograms in which different organisms are located at different axial planes.

## 4. CONCLUSION

The computational processing of DHM holograms significantly depends on the system's optical configuration, which can be extracted from the hologram's spectrum. This work presents a practical guideline to determine the DHM's optical configuration and select the required computational DHM algorithm to provide phase images with minimum phase distortions. All the discussed computational algorithms are publicly available via GitHub. Figure 5 provides the QR codes to access them directly. We aim to offer open-source reconstruction codes for the DHM community using the two most accessible software (i.e., MATLAB and Python).

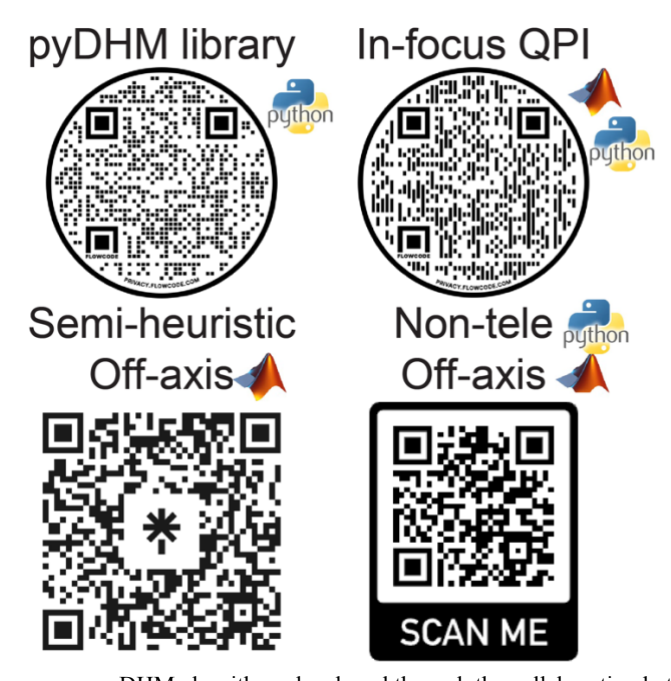


Fig. 5. QR codes to access the open-source DHM algorithms developed through the collaboration between Drs. Trujillo's and Doblas' research team.

## REFERENCES

- 1. G. Popescu, [Quantitative Phase Imaging of Cells and Tissues], McGraw-Hill (2012),
- 2. Park, Y., Popescu, G., Ferraro, F., and Kemper, B., "Quantitative Phase Imaging and Its Applications to Biophysics, Biology, and Medicine," Front. Phys. 7, 2019–2020 (2020). https://www.frontiersin.org/articles/10.3389/fphy.2019.00226/full
- 3. Kim, M. K., "Principles and techniques of digital holographic microscopy," SPIE Reviews 1(1), 18005 (2010).
- 4. Cuche, E., Marquet, P., and Depeursinge, C., "Simultaneous amplitude-contrast and quantitative phase-contrast microscopy by numerical reconstruction of Fresnel off-axis holograms," Appl. Opt. 38(34), 6994–7001 (1999).
- 5. Park, Y. K., Depeursinge, C., and Popescu, G., "Quantitative phase imaging in biomedicine," Nat Photonics **12**(10), 578–589 (2018). https://doi.org/10.1038/s41566-018-0253-x
- 6. Kemper, B., Langehanenberg, P., Bredebusch, I., Schnekenburger, J., and von Bally, G., "Techniques and Applications of Digital Holographic Microscopy for Life Cell Imaging," Proc. SPIE 6633, 66330D (2007). https://doi.org/10.1117/12.728262.
- 7. Lai, Y. W., Krause, M., Savan, A., Thienhaus, S., Koukourakis, N., Hofmann, M. R., and Ludwig, A., "High-throughput characterization of film thickness in thin film materials libraries by digital holographic microscopy," Sci Technol Adv Mater 12(5), 054201 (2011).
- 8. Picazo-Bueno, J. A., Trusiak, M., and Micó, V., "Single-shot slightly off-axis digital holographic microscopy with add-on module based on beamsplitter cube," Opt Express 27(4), 5655 (2019). https://doi.org/10.1364/OE.27.005655
- 9. Madsen, A. G., Panah, M. A., Larsen, P. E., Nielsen, F., and Glückstad, J., "Review of the state-of-the-art of inline holographic microscopy," SPIE Proc. 12436, 124360A (2023). https://doi.org/10.1117/12.2650162.
- 10. Castañeda, R., Trujillo, C., and Doblas, A., "pyDHM: A Python library for applications in digital holographic microscopy," PLoS One 17(10), e0275818 (2022). https://doi.org/10.1371/journal.pone.0275818
- 11. Bogue-Jimenez, B., Trujillo, C., and Doblas, A., "Comprehensive tool for a phase compensation reconstruction method in digital holographic microscopy operating in non-telecentric regime," PLoS One **18**(9), e0291103 (2023). <a href="https://doi.org/10.1371/journal.pone.0291103">https://doi.org/10.1371/journal.pone.0291103</a>.
- 12. Sánchez-Ortiga, E., Doblas, A., Saavedra, G., Martínez-Corral, M., and Garcia-Sucerquia, J., "Off-axis digital holographic microscopy: practical design parameters for operating at diffraction limit," Appl Opt **53**(10), 2058 (2014). https://doi.org/10.1364/AO.53.002058.
- 13. Doblas, A., Sánchez-Ortiga, E., Martínez-Corral, M., Saavedra, G., and Garcia-Sucerquia, J., "Accurate single-shot quantitative phase imaging of biological specimens with telecentric digital holographic microscopy," J Biomed Opt **19**(4), 46022 (2014). https://doi.org/10.1117/1.JBO.19.4.046022.
- 14. Yamaguchi, I., and Zhang, T., "Phase-shifting digital holography," Opt Lett **22**(16), 1268 (1997).
- Trujillo, C., Doblas, A., Saavedra, G., Martínez-Corral, M., and García-Sucerquia, J., "Phase-shifting by means of an electronically tunable lens: quantitative phase imaging of biological specimens with digital holographic microscopy," Opt Lett **41**(7), (2016). <a href="https://doi.org/10.1364/OL.41.001416">https://doi.org/10.1364/OL.41.001416</a>.
- 16. Trujillo, C., and Garcia-Sucerquia, J., "Phase-shifting digital holographic microscopy by using a multi-camera setup," Opt Lett **42**(23), 4841 (2017). <a href="https://doi.org/10.1364/OL.42.004841">https://doi.org/10.1364/OL.42.004841</a>.
- 17. Doblas, A., Buitrago-Duque, C., Robinson, A., and Garcia-Sucerquia, J., "Phase-shifting digital holographic microscopy with an iterative blind reconstruction algorithm," Appl. Opt. **58**(34), G311-G317 (2019). https://doi.org/10.1364/AO.58.00G311.
- 18. Servin, M., Estrada, J. C., Quiroga, J. A., Mosino, J. F., and Cywiak, M., "Noise in phase shifting interferometry," Opt Express 17(11), 8789 (2009). <a href="https://doi.org/10.1364/OE.17.008789">https://doi.org/10.1364/OE.17.008789</a>.
- 19. De Nicola, S., Ferraro, P., Finizio, A., and Pierattini, G., "Wave front reconstruction of Fresnel off-axis holograms with compensation of aberrations by means of phase-shifting digital holography," Opt Lasers Eng 37(4), 331–340 (2002). https://doi.org/10.1016/S0143-8166(01)00087-2.
- Castañeda, R., Buitrago-Duque, C., Garcia-Sucerquia, J., and Doblas, A., "Fast-iterative blind phase-shifting digital holographic microscopy using two images," Appl. Opt. 59(24), 7469-7476 (2020). https://doi.org/10.1364/AO.398352.
- Obando-Vásquez, S., and Trujillo, C., "Computationally efficient phase aberration compensation method for digital holographic microscopy of biological samples," OSA Technical Digest, Biophotonics Congress 2021, paper JW1A.19 JW1A.19 (2021). https://doi.org/10.1364/BODA.2021.JW1A.19.

- 22. Cuche, E., Marquet, P., and Depeursinge, C., "Spatial filtering for zero-order and twin-image elimination in digital off-axis holography," Appl Opt **39**(23), 4070–4075 (2000). https://doi.org/10.1364/AO.39.004070.
- Trujillo, C., Castañeda, R., Piedrahita-Quintero, P., and Garcia-Sucerquia, J., "Automatic full compensation of quantitative phase imaging in off-axis digital holographic microscopy," Appl. Opt. **55**(36), 10299 (2016). https://doi.org/10.1364/AO.55.010299.
- 24. Castaneda, R., and Doblas, A., "Fast-iterative automatic reconstruction method for quantitative phase image with reduced phase perturbations in off-axis digital holographic microscopy," Appl. Opt. **60** (32), 10214 (2021). <a href="https://doi.org/10.1364/AO.437640">https://doi.org/10.1364/AO.437640</a>.
- Obando-Vásquez, S., Doblas, A., and Trujillo, C., "Semi-heuristic phase compensation in digital holographic microscopy for stable and accurate quantitative phase imaging of moving objects," Opt. Laser Eng. 174, 107937 (2024). https://doi.org/10.1016/j.optlaseng.2023.107937.
- 26. Min, J., Yfao, B., Ketelhut, S., Engwer, C., Greve, B., and Kemper, B., "Simple and fast spectral domain algorithm for quantitative phase imaging of living cells with digital holographic microscopy," Opt. Lett. **42**(2), 227–230 (2017). https://doi.org/10.1364/OL.42.000227.
- 27. Cacace, T., Paturzo, M., Memmolo, P., Vassalli, M., Ferraro, P., Fraldi, M., and Mensitieri, G., "Digital holography as 3D tracking tool for assessing acoustophoretic particle manipulation," Opt Express **25**(15), 17746 (2017). https://doi.org/10.1364/OE.25.017746.
- 28. Memmolo, P., Miccio, L., Paturzo, M., Di Caprio, G., Coppola, G., Netti, P. A., and Ferraro, P., "Recent advances in holographic 3D particle tracking," Adv. Opt. Photonics 7(4), 713-755 (2015). https://doi.org/10.1364/AOP.7.000713.
- Piedrahita-Quintero, P., Trujillo, C., and Garcia-Sucerquia, J., "JDiffraction: A GPGPU-accelerated JAVA library for numerical propagation of scalar wave fields," Comput. Phys. Commun. 214, 128-139 (2017). https://doi.org/10.1016/j.cpc.2016.12.016.
- 30. Born, M., and Wolf, E., [Principles of Optics: Electromagnetic Theory of Propagation, Interference and Diffraction of Light], Cambridge University Press, (2005).
- 31. Castaneda, R., Trujillo, C., and Doblas, A., "In-focus quantitative phase imaging from defocused off-axis holograms: synergistic reconstruction framework," Opt Lett **48**(23), 6244 (2023). https://doi.org/10.1364/OL.506400.